JOURNAL OF AIRCRAFT
Vol. 46, No. 2, March–April 2009

Engineering Notes

ENGINEERING NOTES are short manuscripts describing new developments or important results of a preliminary nature. These Notes should not exceed 2500 words (where a figure or table counts as 200 words). Following informal review by the Editors, they may be published within a few months of the date of receipt. Style requirements are the same as for regular contributions (see inside back cover).

Vortex Wake Generated Behind a Forward Swept Wing

T. Lee* and L. S. Ko†
McGill University, Montreal, Quebec H3A 2K6, Canada

DOI: 10.2514/1.39352

Introduction

BECAUSE of its undesirable effects on flight safety and wing aerodynamic performance, the two counter-rotating streamwise tip vortices generated behind aircraft wing tips continue to be of concern to the aviation industry and aerodynamicists. Numerous investigations have been carried out by researchers elsewhere to examine the tip-vortex structure and its dissipation or persistence in both near, intermediate, and far wakes of the wing tips. An excellent review of the airplane trailing vortices and their control is given by Spalart [1]. The majority of the tip-vortex measurements were, however, concentrated on wings with simple rectangular span loading; wing geometries other than a rectangular platform are limited. The tip-vortex flow behind a sweptback and tapered wing was investigated, for example, by Orloff and Cliffone [2], Gold and Visser [3], and Gerontakos and Lee [4]. Gold and Visser [3] also estimated the value of lift-induced drag coefficient of an aft swept and tapered NACA 0012 semiwing of $Re = 1.25 \times 10^5$ by using the wake integral method. Gerontakos and Lee [4] further observed that the inner region of the tip-vortex flow exhibited a self-similar behavior for $x/c_r \geq 2.67$, where x is the streamwise distance downstream from the wing trailing edge, and c_r is the chord of wing root. However, despite published studies on the trailing vortices generated by rectangular wings and sweptback wings, the near-field tip-vortex flow behind a forward-swept and tapered wing is rarely reported.

It should be noted that forward-swept wings are known to perform well at high Mach numbers and have aerodynamic advantages at very low air speeds [5,6]. The boundary layer of a comparable forward-swept wing (FSW) at low air speeds is more stable against attachment line transition and crossflow instability compared to a backward-swept wing (BSW). In addition, air moving over the forward-swept wings tends to flow inward toward the root of the wing instead of outward toward the wing tip as occurs on a backward-swept wing. Breitsamter and Laschka [6] conducted an extensive aerodynamic investigation of a generic 40-deg forward-swept wing model of a NACA 64A10 cross section, with and without an aft swept canard, by using dual-sensor hot-wire probes at $Re = 4.6 \times 10^5$. Detailed surveys of the isocontours of the mean and rms streamwise and lateral velocity flowfields associated with the leading-edge vortex and the tip vortex were presented. The vortex-core flow parameters, including the magnitude of the lift-induced drag, were, however, not reported.

The objective of the present experiment was to investigate the near-field flow characteristics of the tip vortex, generated behind a forward-swept and tapered wing, at $Re = 1.74 \times 10^5$ by using a miniature seven-hole pressure probe. Special attention was given to the effects of downstream distance and airfoil incidence on the behavior and variation of the crossflow and axial velocity distributions, and the strength and size of the tip vortex. The lift-induced drag was also computed and was compared with the wind-tunnel force-balance data. The FSW results were also compared with those of a sweptback wing, of same geometric dimensions, at the same lift coefficient C_L and Re so as to signify the geometric effects of the wing model on the behavior of the tip vortex.

Experimental Apparatus and Methods

The experiment was carried out in the $0.9 \times 1.2 \times 2.7$ m^3 suction-type subsonic wind tunnel at McGill University. A highly polished untwisted forward-swept tapered wing, made of solid aluminum, with an aspect ratio AR of 3.654, a taper ratio of 0.375, a semispan b of 51 cm, and a wing area of 713 cm^2, was used as the test model. The sweep angle at quarter-chord location was set at 24 deg. The root chord c_r was 20.3 cm and the tip chord c_t was 7.6 cm. The square-tipped wing had a NACA 0015 section. The wing model was mounted horizontally at the center of the wind-tunnel test section. A circular endplate of 50 cm diameter with a sharp leading edge was fitted to the one end, located 10 cm from the sidewall of the test section, of the wing model to mitigate the free end effects. The origin of the coordinate system was located at the trailing edge of the tip of the wing with x, y, and z in the streamwise, transverse, and spanwise direction, respectively. The three components of the tip-vortex flow velocities were measured in planes perpendicular to the freestream velocity at eight distances downstream of the wing tip; $x/c_t = 1.5$, 2, 3, 4, 5, 6, 9, and 13 for $\alpha = 9.6$ deg with $C_L = 0.73$ by using a miniature seven-hole pressure probe. Probe traversing was achieved through a custom-built computer-controlled traversing system. The variation of the vortex-core flow parameters with α was also examined for $\alpha = 2$–14 deg at $x/c_t = 6$. Each data plane taken in the near field of the wing models had 33×85 measuring grid points with an increment of $\Delta y = \Delta z = 3.2$ mm (or $1.6\%c_r$), except along the span of the wing where $\Delta z = 6.4$ mm. A finer $\Delta y = \Delta z = 1.6$ mm was also used in the determination of the vortex-core characteristics. The root-chord Reynolds number was fixed at $Re = 1.74 \times 10^5$. For lift and drag measurements, the finite wing model was mounted vertically on an external two-component force balance located below the wind tunnel. The lift-induced drag coefficient C_{Di} ($=D_i/\frac{1}{2}\rho u_o^2 S$, where D_i is the lift-induced drag, u_o is the freestream velocity, and S is wing surface area) was also computed based on the vorticity distributions inferred from the measured crossflow fields and was compared with the wind-tunnel force-balance data. The maximum uncertainty for the experimental data is as follows [4]: mean velocity 3.5%, vorticity component 8%, vortex radius 4%, and velocity fluctuation 3%. The uncertainty in C_L and C_D determinations were ± 0.01 and ± 0.007, respectively.

Received 25 June 2008; revision received 10 September 2008; accepted for publication 12 September 2008.

*Associate Professor, Department of Mechanical Engineering. AIAA Member.

†Research Assistant, Department of Mechanical Engineering.

Results and Discussion

Figure 1 summarizes the evolution of the normalized vortex-core flow parameters, including the total circulation Γ_o, as it progressed downstream (for $1.5 \leq x/c_t \leq 13$) at $\alpha = 9.6$ deg (or $C_L = 0.73$). Also included in this figure are the BSW measurements at the same lift coefficient and Re. Note that for $x/c_t < 4$, the vortex-core values of the FSW were circumferentially averaged values. The peak tangential velocity $v_{\theta\text{peak}}$ and peak vorticity ζ_{peak} of the tip vortex behind the FSW were found to be generally decreased with x/c_t (Figs. 1a and 1b), whereas the core radius r_c (defined at which v_θ is a maximum) and core circulation Γ_c were increased (Figs. 1c and 1d). The circulation, or vortex strength, was calculated by a line integral, which was evaluated by repeated applications of the trapezoidal rule and was performed on either circular paths or paths of constant vorticity. The observed decrease in ζ_{peak} as the vortex traveled downstream during the roll-up process can be attributed to the net balance between the continuous trapping of the vorticity from the shear layer, which tends to increase the magnitude of ζ_{peak} with distance, and the diffusion of vorticity by viscosity and turbulence, which tends to decrease it. The decrease in $v_{\theta\text{peak}}$ and ζ_{peak}, and the increase in r_c and Γ_c of the FSW were of a much less degree, compared with those of the BSW, and always had a reduced value, as a result of the inward- and outward-going spanwise flows associated with the FSW and BSW models, respectively.

Figures 1e and 1f show that, for the FSW, the total circulation Γ_o and the outer radius r_o (i.e., the radius at which the circulation $\Gamma(r_o)$ reached 95% of Γ_o) were also increased with increasing x/c_t, except for $x/c_t > 9$. A large drop in the magnitude of Γ_o and r_o was, however, noticed at $x/c_t = 13$. The BSW exhibited a higher Γ_o and r_o compared with the FSW at the same C_L and Re, as a result of the thicker shear layers of a higher vorticity level compared to that of the FSW. Furthermore, for $x/c_t > 6$, the distribution of circulation $\Gamma(r)$ of the inner flow region became nearly axisymmetric, which followed a $\Gamma \propto r^2$ profile for $r/r_c < 0.4$ and varied logarithmically for $0.5 < r/r_c < 1.4$. The observed self-similar behavior of the inner region of a nearly axisymmetric tip vortex in the near field is of particular interest because it generally takes a distance of several tens or even hundreds of wing chords downstream for the vortex to become fully developed and attain the characteristics of asymptotic trailing vortices [7,8]. The results also show that the vortex-core axial velocity u_c of the FSW remained virtually unchanged (with $u_c \approx 0.85u_o$; Fig. 1g), regardless of the downstream distance. In

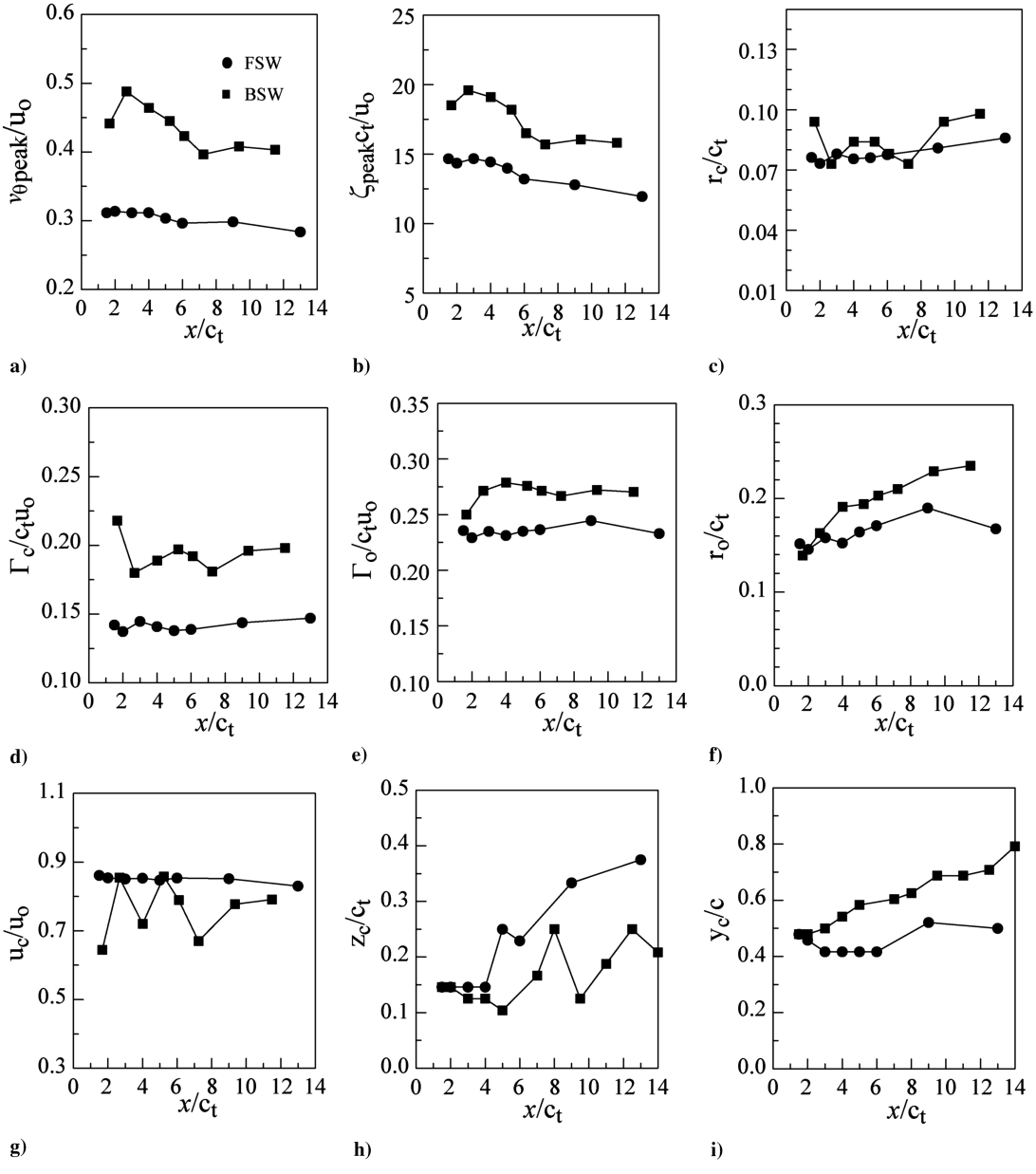

Fig. 1 Variation of vortex flow parameters with x/c for $C_L = 0.73$.

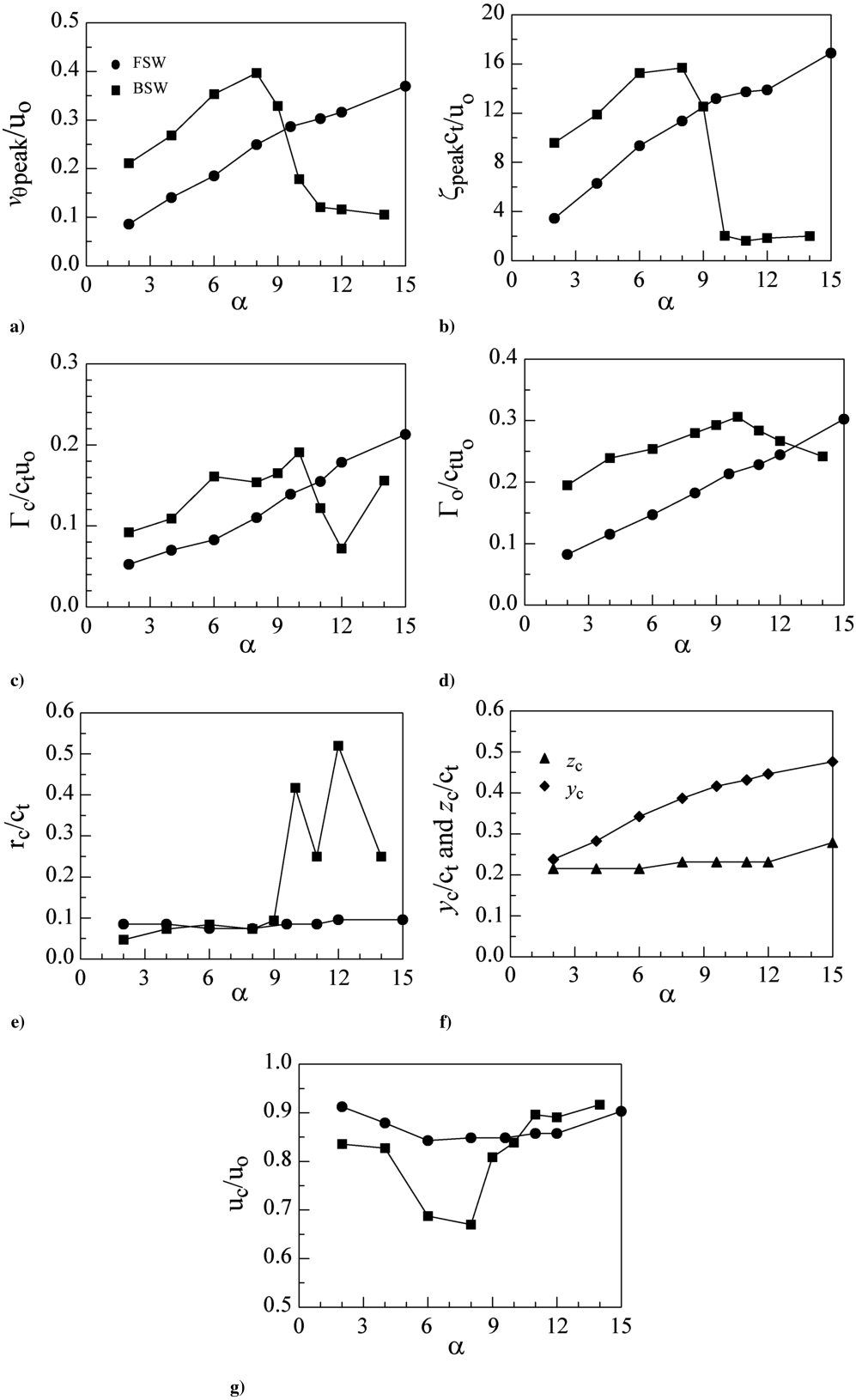

Fig. 2 Variation of vortex-core flow parameters with α at $x/c_t = 6$.

contrast to the FSW, a large variation in the u_c of the BSW (for $x/c_t \leq 9$) was, however, observed. A more in-depth discussion of the vortex structure of the BSW is given by Gerontakos and Lee [4]. The vortex trajectory of the FSW had an inboard and upward movement as the vortex progressed downstream (Figs. 1h and 1i). The vortex center was, however, found to be located further below the wing trailing edge and inboard toward the wing root compared to that of the BSW.

The variation of the vortex-core flow parameters with α at $x/c_t = 6$ was also investigated and is summarized in Fig. 2. The normalized $v_{\theta peak}$, ζ_{peak}, Γ_c, and Γ_o of the FSW were found to increase linearly with α for α up to 15 deg (larger than the static-stall angle

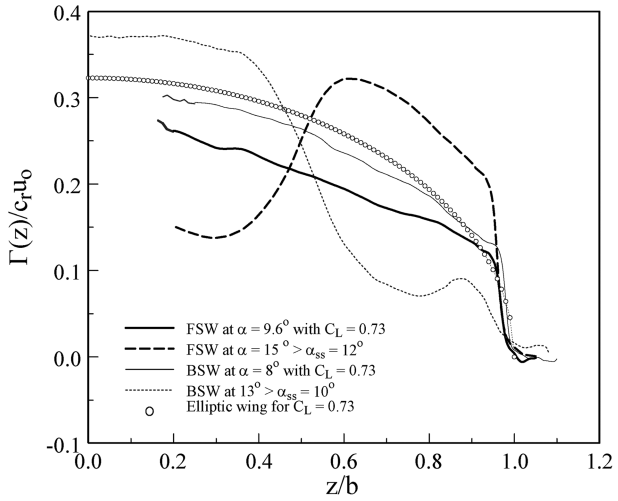

Fig. 3 Spanwise circulation distribution.

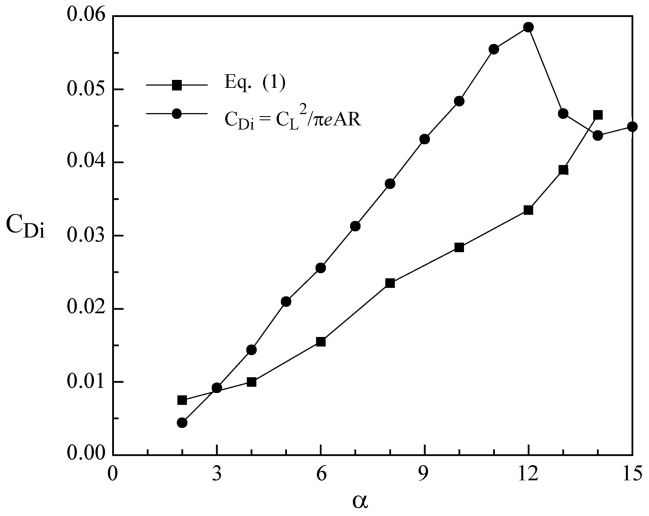

Fig. 4 Variation of lift-induced drag coefficient with α.

$\alpha_{ss} = 12$ deg; Figs. 2a–2d), as a result of the lift stall initiated in the root region, which consequently leaves the tip vortex formed at the wing tip unaffected. In contrast to the continuous increase in $v_{\theta\text{peak}}$, ζ_{peak}, and the vortex strength of the FSW, the value of Γ_c and Γ_o of the BSW, however, exhibited a local maximum at $\alpha = \alpha_{ss} = 10$ deg, due to the lift stall initiated in the tip region of the wing. The normalized value of $v_{\theta\text{peak}}$ and ζ_{peak} also experienced a rapid drop between $\alpha = 8$ and 10 deg. The vortex-core flow parameters of the BSW had a higher value than the FSW, due to the spanwise flow in the outboard direction and the subsequent thickening of the boundary layer as the flow traveled toward the tip, and increased linearly with α before the local maximum was attained. A significantly lowered $v_{\theta\text{peak}}$, ζ_{peak}, and Γ_c for $\alpha > \alpha_{ss} \approx 10$ deg of the BSW, compared with the FSW, was noticed. The tip stall characteristic of the BSW also rendered a more diffused tip vortex of a dramatically increased vortex-core size (for $\alpha > \alpha_{ss}$) compared with that of the FSW (Fig. 2e). The core radius of the FSW, however, remained basically unaffected (with r_c of about $8\% c_t$) even for $\alpha > \alpha_{ss}$. Also, the vortex center of the FSW was shifted slightly inboard but further above the wing trailing edge with increasing α (Fig. 2f). The vortex-core axial velocity u_c of the FSW was found to vary slightly between 0.91 and $0.85u_o$ for $\alpha = 2$–14 deg tested (Fig. 2g). In contrast, the u_c of the BSW decreased considerably for low α (for $\alpha \leq 6$ deg), remained virtually unchanged (for $6 \leq \alpha \leq 8$ deg), and was followed by a sharp rise in the vicinity of the stall angle.

The behavior of the vortex-core flow parameters of the FSW, in comparison to those of the BSW, can also be reflected from the spanwise circulation $\Gamma(z)$ distributions at $x/c_t = 6$ (Fig. 3). Figure 3 shows that there was a dip in the $\Gamma(z)$ distribution in the tip region, regardless of the wing planform, compared to that of an elliptic wing (denoted by the open circle). The near-tip $\Gamma(z)$ distribution became more precipitous and shifted further inboard with a drastically increased Γ level close to the root of the wing model for $\alpha > \alpha_{ss}$. At the same lift condition, the $\Gamma(z)$ distribution near the tip was more gradual for the FSW compared with that of BSW. At $C_L = 0.73$, an extrapolated normalized root circulation $\Gamma_b/c_t u_o$ of about 0.29 and 0.31 can be obtained for the FSW and BSW, respectively, which translates into a Γ_o/Γ_b ratio of about 83 and 86%, suggesting that, in the near wake (at $x/c_t = 6$ and $C_L = 0.73$), about 83 and 86% of Γ_b was entrained into the tip-vortex flow for the two wing planforms considered. The discrepancy in the stalling mechanisms can also be reflected from the pronounced reduction in $\Gamma(z)$ in the root and tip regions (denoted by dashed and dotted lines, respectively) for the FSW and BSW, respectively, for $\alpha > \alpha_{ss}$.

The vorticity inferred from the measured crossflow velocity field was also used to compute the lift-induced drag by using the Maskell induced-drag model [9]. The crossflow velocity vectors within the measurement plane were decomposed into a stream function $\psi(y, z)$ and a crossflow velocity potential $\phi(y, z)$ with the imposed boundary conditions requiring both ψ and $\partial\phi/\partial n$ to be zero on the walls of the wind tunnel. The lift-induced drag D_i was then obtained by (as suggested by Brune [10] and Kusunose [11])

$$D_i = \frac{1}{2}\rho_\infty \int_{S_\zeta} \int \psi\zeta \, \mathrm{d}y \, \mathrm{d}z - \frac{1}{2}\rho_\infty \int_{S_1} \int \phi\sigma \, \mathrm{d}y \, \mathrm{d}z \qquad (1)$$

where $\zeta = \partial w/\partial y - \partial v/\partial z$ is the streamwise vorticity, the surface S_ζ is the region within S_1 where the vorticity is nonzero, and $\sigma = \partial v/\partial y + \partial w/\partial z = -\partial u/\partial x$ is a source term that is small outside the viscous wake. The value of C_{Di} of the FSW was found to increase rather nonlinearly with α (Fig. 4). The C_{Di} computed was, however, found to be persistently below that estimated by the simple $C_{Di} = C_L^2/\pi e\mathrm{AR}$ expression, except for $\alpha < 4$ and $\alpha > 12$ deg. The C_{Di} estimated (denoted by the filled circle) was found to increase with α up to α_{ss}, and began to decrease with increasing α for $\alpha > \alpha_{ss}$.

Conclusions

The near-field tip-vortex flow behind a forward-swept and tapered wing at $Re = 1.74 \times 10^5$ was investigated. The vortex-core flow parameters became streamwise-invariant and nearly axisymmetric for $x/c_t > 4$. The vortex flow parameters, except for the core radius and the core axial velocity, were found to increase linearly with increasing α. No significant variation in the core radius and axial velocity with α was observed. In contrast to the FSW, the $v_{\theta\text{peak}}$ and ζ_{peak} and the vortex strength of the BSW were found to increase with α up to α_{ss}, and began to decrease with a further increase in α. The C_{Di}, computed via the Maskell model [9], was found to increase, in a somewhat quadratic form, with increasing α, and was of lower value than that predicted by the simple $C_{Di} = C_L^2/\pi e\mathrm{AR}$ expression. The C_{Di} estimated by the Prandtl's simple expression can, however, serve as an upper bound of C_{Di} estimation for low Reynolds number flows in which the viscous effects become dominant and boundary-layer flow separation is unavoidable.

References

[1] Spalart, P. R., "Airplane Trailing Vortices," *Annual Review of Fluid Mechanics*, Vol. 30, Jan. 1998, pp. 107–138. doi:10.1146/annurev.fluid.30.1.107

[2] Orloff, K. L., and Cliffone, D. L., "Vortex Measurements Behind a Swept Wing Transport Model," *Journal of Aircraft*, Vol. 11, No. 6, 1974, pp. 362–364. doi:10.2514/3.59259

[3] Gold, N., and Visser, K., "Aerodynamic Effects of Local Dihedral on a Raked Wingtip," AIAA Paper 2002-0831, 2002.

[4] Gerontakos, P., and Lee, T., "Near-Field Tip Vortex Behind a Swept and Tapered Wing Model," *Experiments in Fluids*, Vol. 40, No. 1, 2006, pp. 141–155. doi:10.1007/s00348-005-0056-y

[5] Herbst, W. B., "Future Fighter Technologies," *Journal of Aircraft*, Vol. 17, No. 8, 1980, pp. 561–566. doi:10.2514/3.44674

[6] Breitsamter, C., and Laschka, B., "Vortical Flowfield Structure at Forward Swept-Wing Configurations," *Journal of Aircraft*, Vol. 38, No. 2, 2001, pp. 193–207. doi:10.2514/2.2758

[7] Hoffmann, E. R., and Joubert, P. N., "Turbulent Line Vortices," *Journal of Fluid Mechanics*, Vol. 16, No. 3, 1963, pp. 395–411. doi:10.1017/S0022112063000859

[8] Phillips, W. R. C., "The Turbulent Trailing Vortex During Roll-Up," *Journal of Fluid Mechanics*, Vol. 105, 1981, pp. 451–467. doi:10.1017/S0022112081003285

[9] Maskell, E., "Progress Towards a Method for the Measurement of the Components of the Drag of a Wing of Finite Span," Royal Aircraft Establishment TR 72232, 1973.

[10] Brune, G. W., "Quantitative Low-Speed Wake Surveys," *Journal of Aircraft*, Vol. 31, No. 2, 1994, pp. 249–255. doi:10.2514/3.46481

[11] Kusunose, K., "Drag Reduction Based on a Wake-Integral Method," AIAA Paper 98-2723, 1998.